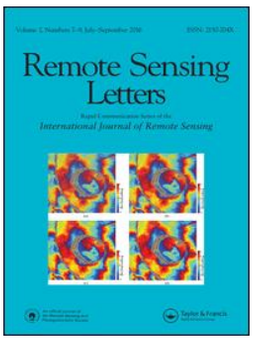

Remote Sensing Letters

ISSN: (Print) (Online) Journal homepage: https://www.tandfonline.com/loi/trsl20

A novel truncated nonconvex nonsmooth variational method for SAR image despeckling

Mingqiang Guo , Chengde Han , Weina Wang , Saishang Zhong , Ruina Lv & Zheng Liu

To cite this article: Mingqiang Guo , Chengde Han , Weina Wang , Saishang Zhong , Ruina Lv & Zheng Liu (2021) A novel truncated nonconvex nonsmooth variational method for SAR image despeckling, Remote Sensing Letters, 12:2, 174-183

To link to this article: https://doi.org/10.1080/2150704X.2020.1846820

Published online: 10 Dec 2020.

REMOTE SENSING LETTERS
2020, VOL. 12, NO. 2, 174–183
https://doi.org/10.1080/2150704X.2020.1846820

Taylor & Francis
Taylor & Francis Group

A novel truncated nonconvex nonsmooth variational method for SAR image despeckling

Mingqiang Guo[a], Chengde Han[b], Weina Wang[c], Saishang Zhong[d], Ruina Lv[b] and Zheng Liu[a]

[a]School of Geography and Information Engineering, National Engineering Research Center of Geographic Information System, China University of Geosciences, Wuhan, China; [b]School of Geography and Information Engineering, China University of Geosciences, Wuhan, China; [c]Department of Mathematics, Hangzhou Dianzi University, Hangzhou, China; [d]School of Earth Resources, State Key Laboratory of Geological Processes and Mineral Resources, China University of Geosciences, Wuhan, China

ABSTRACT

Speckle reduction is a fundamental problem in coherent imaging systems. In this paper, to suppress the speckle in SAR images, we propose a novel truncated nonconvex nonsmooth model. It incorporates a truncated nonconvex regularization term and an I-divergence fidelity term. The truncated ℓ_p norm $(0 < p < 1)$ regularization can better recover neat edges and simultaneously prevent contrast reduction artefact. The I-divergence fidelity term is used to suppress the multiplicative noise effectively. We also propose an efficient algorithm based on variable-splitting and alternating direction method of multipliers (ADMM) method to solve the model. Compared to state-of-the-art speckle suppression methods, intensive experimental results on a variety of SAR images show the superiority of the proposed method qualitatively and quantitatively.

ARTICLE HISTORY
Received 25 July 2020
Accepted 28 October 2020

1. Introduction

Synthetic aperture radar (SAR) has attracted considerable attention because of its advantages, such as high spatial resolution and all-day, all-weather imaging capability. As coherent imaging systems, speckle noise inevitably appears in SAR images, which keeps us from interpreting valuable information such as texture (Yu et al. 2020a), edges (Yu et al. 2020b), and point targets (He et al. 2020). Therefore, despeckling is critical in SAR images. Over the years, state-of-the-art methods have been proposed for speckle suppression in SAR images. Generally, we classify existing despeckling methods into two major categories as follows.

1.1. Nonlocal filtering methods

Nonlocal filtering methods, e.g., nonlocal mean (NLM) (Buades, Coll, and Morel 2005), block-matching 3D (BM3D) (Dabov et al. 2007), overlapping group sparsity (Liu et al. 2015), and low-rank recovery (Dong, Shi, and Li 2013), are originally proposed to recover pattern similarity patches of natural images corrupted by additive Gaussian noise. Inspired by the great success

CONTACT Zheng Liu liu.zheng.jojo@gmail.com School of Geography and Information Engineering, National Engineering Research Center of Geographic Information System, China University of Geosciences, Wuhan 430074, China

of these nonlocal methods for removing additive noise, extensive works extended these methods to suppress speckle noise in SAR images. An extension of NLM for despeckling is proposed by designing an efficient similarity measure and an iterative strategy (Deledalle, Denis, and Tupin 2009). The overlapping group sparsity regularization with the I-divergence data fidelity is used for despeckling (Liu et al. 2016). A SAR version of BM3D is presented by altering the original BM3D major steps for fitting the peculiarities of SAR images (Parrilli et al. 2011). Low-rank methods based on nuclear norm minimization (Guan et al. 2018; Liu et al. 2018; Guan et al. 2019; Chen et al. 2019) were also adopted in SAR images. As we can see, the self-similarity of the natural image is employed in these nonlocal-based methods, so the breakthrough performance usually is guaranteed in SAR images for despeckling. However, because of the attempt to recognize similar structures even when they are absent, some annoying artefacts appear in homogeneous regions of the despeckling result for these nonlocal methods.

1.2. Variational methods

Due to the good performance for preserving edges and recovering homogeneous regions, variational methods have been widely used in image processing. The aim of variational methods is to minimize some energy functions which include a data fitting and regularization term. A model based on maximum a posteriori (MAP), abbreviated as the AA model, is proposed to remove multiplicative noise well (Aubert and Aujol 2008). They adopted gradient descent approach to solve the AA model, whereas their approach cannot find the global minimum because of the nonconvex property of the AA model. In order to tackle this problem, many researchers have done a lot of works. Some studies introduced the logarithmic transformation of the AA model (Feng, Lei, and Gao 2014). However, due to the nonlinear property of the logarithmic transformation, the values in darkness of the image are expanded while those in the brightness are compressed. In order to tackle this problem, the classical convex I-divergence model is proposed (Steidl and Teuber 2010), which does not require the deficiency of the logarithmic transformation. To reduce staircase artefacts of TV regularization term, many high-order methods (Chan, Marquina, and Mulet 2000; Lysaker, Lundervold, and Tai 2003; Shi et al. 2019; Xiang et al. 2019) are proposed. A high-order total variation regularizer with the I-divergence data fitting term is proposed for despeckling in SAR images (Liu et al. 2013).

As we have seen, the aforementioned state-of-the-art methods have some problems in suppressing the speckle in SAR images or are less robust for preventing unnatural artefacts such as ghost artefacts, smooth brushstrokes, and contrast reduction in despeckling results. To tackle these problems, we propose a novel truncated nonconvex nonsmooth variational model, consisting of a regularization and fidelity term, to suppress the speckle in SAR images. The ℓ_p regularization term with a truncated function demonstrates good edge-preserving, homogeneity-recovering, and contrast-preserving abilities. The convex I-divergence fidelity term is robust for suppressing multiplicative noise. We also propose an efficient algorithm to solve the proposed model. Specifically, the main contributions of the paper are summarized as follows:

- A novel truncated nonconvex nonsmooth variational model is presented for speckle suppression in SAR images. It is able to preserve neat edges, recover homogeneous regions well, and prevent contrast reduction effects.
- To solve the proposed truncated nonconvex model, an efficient algorithm is developed based on variable-splitting and alternating direction method of multipliers (ADMM) method.
- Compared to state-of-the-art methods, intensive experimental results show that the proposed method demonstrates favourably speckle suppression and contrast preserving effects.

2. Methodology

We first define some basic function spaces and discrete associated operators in this section. Then, our truncated nonconvex nonsmooth model and the corresponding solving algorithm are proposed.

2.1. Basic notation

Assume the SAR image intensity u to be represented as an $\mathrm{M} \times \mathrm{N}$ matrix, we denote the Euclidean space $\mathbb{R}^{\mathrm{M}\times\mathrm{N}}$ as V. The discrete gradient operator is a mapping $\nabla : V \to Q$, where $Q = V \times V$. For $u \in V$, ∇u is given by

$$(\nabla u)_{i,j} = ((D_x^+ u)_{i,j}, (D_y^+ u)_{i,j}),$$

where $i = 1, \ldots, \mathrm{M}, j = 1, \ldots, \mathrm{N}$ is the pixel position of the SAR image intensity u. D_x^+ and D_y^+ are respectively horizontal and vertical forward difference operators with periodic boundary condition. The inner product and norm in space V and Q are as follows:

$$\begin{aligned} &\langle u^1, u^2\rangle_V = u^1 \cdot u^2, \quad \|\nabla u\|_V = \sqrt{\langle \nabla u, \nabla u\rangle_V}, \qquad u, u^1, u^2 \in V, \\ &\langle p, q\rangle_Q = \langle p_1, q_1\rangle_V + \langle p_2, q_2\rangle_V, \quad \|p\|_Q = \sqrt{\langle p, p\rangle_Q}, \qquad p, q \in Q. \end{aligned}$$

2.2. Truncated ℓ_p-regularized model and corresponding numerical algorithm

Speckle noise in SAR images is usually regarded as multiplicative noise, as follows:

$$f = u\eta, \tag{1}$$

where $f \in V$ is the observed SAR image intensity, u is the underlying true image intensity, and η is assumed as speckle noise that follows a Gamma distribution. The probability density function of η for the L-look SAR image is given by the following Gamma distribution:

$$\mathrm{P}(\eta) = \frac{1}{\Gamma(\mathrm{L})}\mathrm{L}^{\mathrm{L}}\eta^{\mathrm{L}-1}e^{-\mathrm{L}\eta}\mathrm{H}(\eta), \tag{2}$$

where Γ is the classical Gamma function, and H is a Heaviside function.

Given the observed SAR image intensity $f \in V$, we proposed the following truncated nonconvex nonsmooth variational model

$$\min_{u\in V}\{a(u-f\log u)+\sum_{1\le i\le \mathrm{M},1\le j\le \mathrm{N}}\mathcal{T}(\|(\quad u)_{i,j}\|^p)\},\tag{3}$$

where $\|(\quad u)_{i,j}\|^p=(\sqrt{(D_x^+u)_{i,j}^2+(D_y^+u)_{i,j}^2})^p$, a is a non-negative parameter balancing the influences of the regularization and fidelity term. p is a tuning parameter in the range of $(0,1)$, which is used to control the degree of nonconvexity of the ℓ_p regularizer. $\mathcal{T}(\|(\quad u)_{i,j}\|^p)=min(\|(\quad u)_{i,j}\|^p,\tau^p)$ is a truncated function with the threshold τ, which is a positive real parameter.

Because of the problem (3) is nonsmooth and nonconvex, it is challenging to directly solve it. The strategy of variable-splitting and ADMM is adopted to solve the nonconvex $TV_p-\ell_2$ model successfully (Lanza, Morigi, and Sgallari 2016). Hence, using of the same strategy, we first introduce two auxiliary variables t and w and reformulate the problem (3) as:

$$\begin{aligned}&\min_{u\in V,w\in V,t\in Q}\{\ a(w-f\log w)+\sum_{1\le i\le \mathrm{M},1\le j\le \mathrm{N}}\mathcal{T}(\|\ t_{i,j}\|^p)\}.\\&\text{s.t. } w=u,t=\quad u\end{aligned}\tag{4}$$

The augmented Lagrangian equation of (4) is as follows:

$$\begin{aligned}\mathcal{L}(u,t,w;\lambda_t,\lambda_w)\ =\ \ &a(w-f\log w)+\sum_{1\le i\le \mathrm{M},1\le j\le \mathrm{N}}\mathcal{T}(\|\ t_{i,j}\|^p)+\langle\lambda_t,t-\quad u\rangle_Q+\langle\lambda_w,w-u\rangle_V\\&+\tfrac{r_t}{2}\|\ t-\quad u\ \|_Q^2+\tfrac{r_w}{2}\|\ w-u\ \|_V^2,\end{aligned}\tag{5}$$

where r_t,r_w are positive penalty coefficients, and λ_t,λ_w are Lagrange multipliers. The primal variables update procedure can be separated into three subproblems. The alternating minimization procedure for solving (3) is sketched in Algorithm 1. The iteration procedure terminates when one of the stopping criteria is satisfied.

Algorithm 1 Solving truncated nonconvex nonsmooth variational model (3)

Input: f,a,τ,p,r_t,r_w;

Initialization: $w^0=f,u^0=f,\lambda_t^0=0,\lambda_w^0=0,k=0,K=500,\varepsilon=1e^{-4}$;

Repeat

(1)Solve t-subproblem

For fixed (u^k,λ_t^k), compute t^{k+1} according to Algorithm 2;

(2)Solve w-subproblem

For fixed (u^k,λ_w^k), compute w^{k+1} according to (13);

(3)Solve u-subproblem

For fixed $(t^k,w^k,\lambda_w^k,\lambda_t^k)$,compute u^{k+1} according to (15);

(4)Update Lagrange multiplier

$$\lambda_t^{k+1}=\lambda_t^k+r_t(t^{k+1}-\quad u^{k+1});$$

$$\lambda_w^{k+1}=\lambda_w^k+r_w(w^{k+1}-u^{k+1});$$

until $\|\ u^{k+1}-u^k\ \|_V^2<\varepsilon$ or $k>K$

Output: u^k.

(1). t-subproblem. The t sub-minimization problem can be written as:

$$\min_{t\in Q} \sum_{1\le i\le \mathrm{M}, 1\le j\le \mathrm{N}} \mathcal{T}(\| t_{i,j}\|^p) + \frac{r_t}{2} \| t - (\ u - \frac{\lambda_t}{r_t}) \|_Q^2 . \tag{6}$$

Note that the problem (6) can be spatially decomposed in explicit component-wise form at each pixel. Thus, for each $t_{i,j}$, we only need to solve the following problem:

$$\min_{t_{ij}\in Q} \ \mathcal{T}(\| t_{ij}\|^p) + \frac{r_t}{2} \| t_{ij} - q_{ij}\|^2, \tag{7}$$

with the constant vectors $q_{i,j}$ defined as:

$$q_{i,j} = (\ u)_{i,j} - \frac{(\lambda_t)_{i,j}}{r_t}. \tag{8}$$

And the solution of Equation (7) has been proven in (Wu, Liu, and Wen 2018). Here, we just give the result, which is expressed in Algorithm 2. For the sake of readability of Algorithm 2, two functions are first defined as follows:

$$\chi_1(s) = s^p + \frac{r_t}{2}(s - \| q_{i,j} \|)^2, \ \ \chi_2(s) = \tau^p + \frac{r_t}{2}(s - \| q_{i,j} \|)^2. \tag{9}$$

The first and second-order derivatives of $\chi_1(s)$ are as follows:

$$\chi_1^{'}(s) = ps^{p-1} + r_t(s - \| q_{i,j} \|), \ \chi_1^{''}(s) = p(p-1)s^{p-2} + r_t. \tag{10}$$

Assume s_L is the root of $\chi_1^{''}(s) = 0$, and we have $s_L = (\frac{p(p-1)}{r_t})^{\frac{1}{2-p}}$.

Algorithm 2 Find the global minimizer of Equation (7)

Input: $q_{i,j}, \tau, p, r_t, s_L$;
(1) find the minimizer of $s_1^* = \min_{0\le s\le\tau}\{\chi_1(s)\}$.
if $\chi_1^{'}(s_L+) < 0$ **then**
find the root $\bar{s}$ of equation $\chi_1^{'}(s) = 0$ in $[s_L, \| q_{i,j} \|]$;
set the feasible set $\chi = \{0, \min(\bar{s}, \tau)\}$;
choose $s_1^* \in \chi$ with $s_1^* = \min_{s\in\chi}\chi_1(s)$;
else
set $s_1^* = 0$;
(2) find the minimizer of $s_2^* = \min_{\|q_{i,j}\|\le\tau}\chi_2(s)$.
set $s_2^* = \max(\tau, \| q_{i,j} \|)$;
(3) find the global minimizer s^*.
Choose s^* with

$$s^* = \begin{cases} s_1^*, & \chi_1(s_1^*) < \chi_2(s_2^*), \\ \{s_1^*, s_2^*\}, & \chi_1(s_1^*) = \chi_2(s_2^*), \\ s_2^*, & \text{otherwise.} \end{cases}$$

Output: $t_{i,j} = \frac{s^*}{\|q_{i,j}\|} q_{i,j}$.

(2) w-subproblem. The w-subproblem can be written as:

$$\min_{\mathrm{w}\in\mathrm{V}} a(w - f\log w) + \langle \lambda_w, w - u\rangle_V + \frac{r_w}{2} \| w - u \|_V^2 . \tag{11}$$

Since the minimization problem in (11) is strictly convex, which can be easily solved by first-order optimality conditions, as below:

$$w^2 + (\frac{a}{r_w} + \frac{\lambda_w}{r_w} - u)w - \frac{a}{r_w} f = 0. \tag{12}$$

It is obvious that Equation (12) has an explicit solution as follows:

$$w = \frac{\sqrt{4(\frac{a}{r_w} f) + (\frac{a}{r_w} + \frac{\lambda_w}{r_w} - u)^2} - (\frac{a}{r_w} + \frac{\lambda_w}{r_w} - u)}{2}. \tag{13}$$

(3) u-subproblem. The u-subproblem can be reformulated as:

$$\min_{u \in V} \frac{r_t}{2} \| \quad u - (t + \frac{\lambda_t}{r_t}) \|_Q^2 + \frac{r_w}{2} \| u - (w + \frac{\lambda_w}{r_w}) \|_V^2 . \tag{14}$$

As we can see, the problem (14) is a quadratic minimization problem. The problem has first-order optimality conditions.

$$^T \quad u + \frac{r_w}{r_t} u = \quad ^T(t^k + \frac{\lambda_t^k}{r_t}) + \frac{r_w}{r_t}(w^k + \frac{\lambda_w^k}{r_w}). \tag{15}$$

In this paper, the matrix is a difference operator with periodic boundary conditions. So ^{T} is the block circulant matrix with circulant blocks, the coefficient matrix in (15) can be diagonalized by the 2D discrete Fourier transform (FFT implementation).

3. Numerical experiments

In this section, numerical experiments on two real SAR images are presented in Figures 1(a) and 2(a) to demonstrate the performance of our despeckling method. The two TerraSAR images are amplitude format with size 512 $\times$ 512, which can be accessed from https://www.intelligence-airbusds.com. The Band, Polarization Configuration, Polarization Mode, and Minimum Resolution of SAR1 and SAR2 are X, Single-Polarization, HH, and 5 m, respectively. The Imaging Mode of SAR1 and SAR2 are High Resolution SpotLight and StripMap, respectively. SAR1 was obtained in Pima County, Arizona, USA on 23 December 2010, and SAR2 was obtained in Three Gorges Dam, Hubei, China on 21 October 2009. For testifying the abilities of preserving neat edges and recovering homogeneous regions, the indexes of equivalent number of looks (ENL) (Xie, Pierce, and Ulaby 2002) and edge preservation index (EPI) (Sattar et al. 1997) are adopted with SAR1 and SAR2. The ENL of the above two real SAR images were

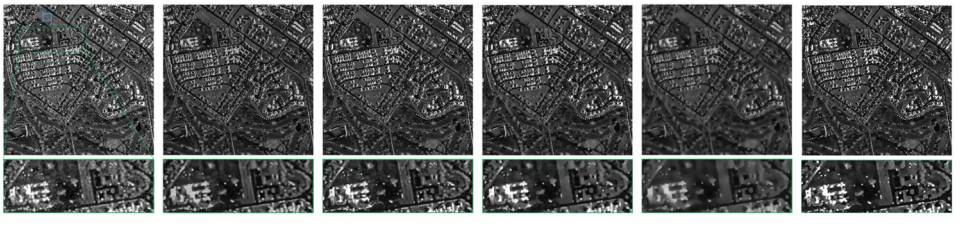

(a) SAR1 (b) SARBM3D (c) PPBit (d) DCA (e) TGV (f) TRTVpIdiv

Figure 1. Despeckling results of SAR1. From left to right: noisy input, results produced by SARBM3D, PPBit, DCA, TGV, and TRTVpIdiv($a = 11, p = 0.4, \tau = 3$), respectively. The zoomed views, showed in the second row.

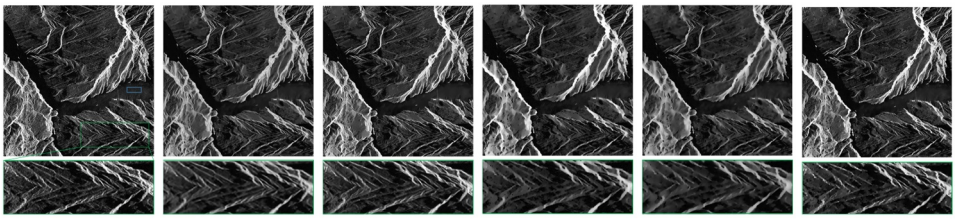

(a) SAR2 (b) SARBM3D (c) PPBit (d) DCA (e) TGV (f) TRTVpIdiv

Figure 2. Despeckling results of SAR2. From left to right: noisy input, results produced by SARBM3D, PPBit, DCA, TGV, and TRTVpIdiv($\alpha = 12, p = 0.5, \tau = 3$), respectively. The zoomed views, showed in the second row.

estimated from the homogenous regions in the blue rectangles in Figures 1(a) and 2(a). The range of EPI is [0,1], and EPI will be close to 1 when edges are preserved well during despeckling process. The ratio images are adopted in Figure 3 to measure the ability of the structure retaining (Meng et al. 2018). State-of-the-art approaches including DCA (Li, Lou, and Zeng 2016), TGV (Feng, Lei, and Gao 2014), PPBit (Deledalle, Denis, and Tupin 2009), and SARBM3D (Parrilli et al. 2011) are adopted to provide quantitative and visual comparisons. Our truncated nonconvex nonsmooth method is abbreviated as TRTVpIdiv. We have implemented TGV (Feng, Lei, and Gao 2014) according to the published paper using Matlab. For the other tested methods, we perform the code provided by their authors. All of the examples are run on a laptop with an Intel i5 core 2.6 GHz processor and 8GB RAM by using Matlab R2017b.

As we know, most variational methods have parameters, which need to be manually tuned. Our truncated nonconvex nonsmooth variational model (3) has three parameters: α, p, and τ. These three parameters have different roles and should be tuned to produce satisfactory results. Specifically, α is a tradeoff between the regularization and fidelity term. It is introduced to prevent the solution deviating far from the input. If α is too large, the noise cannot be removed cleanly; and if α is too small, the fine features will be oversmoothed. To produce satisfactory results, we empirically set α in the range of [0.1, 20] for $L = 1$ and 2, and [10, 100] for $L > 2$. p is used to control the degree of nonconvexity of the ℓ_p regularization of the proposed model (3). Too strong nonconvexity will sharpen features and result in staircase effects. In

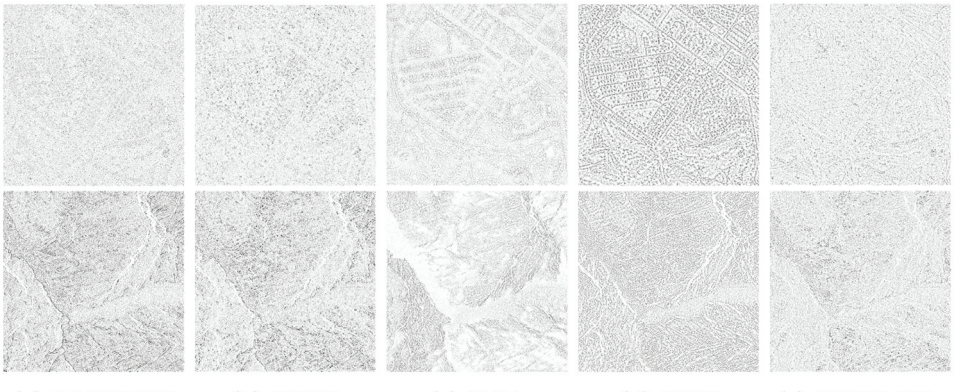

(a) SARBM3D (b) PPBit (c) DCA (d) TGV (e) TRTVpIdiv

Figure 3. First to second rows are the ratio images for SAR1 and SAR2, respectively. From left to right: ratio images produced by SARBM3D, PPBit, DCA, TGV, and TRTVpIdiv, respectively.

contrast, too weak nonconvexity will yield a result with blurred features. Thus, p is suggested to be set in the range of [0.1, 0.6] for cartoon images, and [0.4, 0.9] for images including rich details. We use τ to improve the image contrast. We first set τ in the range of [1, 5], and then gradually increase it for higher values of ENL and EPI.

In Figure 1, we compare the despeckling results produced by the tested methods. For all of the test methods, we carefully tune their parameters for yielding the best despeckling results. As we can see, all of the tested methods can effectively suppress speckle. However, DCA and TGV blur and flatten features more or less, especially for TGV for its second derivative property; see Figure 1(d,e). In Figure 3(c,d), the corresponding ratio images of DCA and TGV contain obvious structures, which means that they retain poor detail. Furthermore, PPBit suffers from brushstrokes, and SARBM3D undergoes ghost artefacts, in some homogeneous regions; see Figure 1(c,b). In the corresponding ratio images, PPBit, SARBM3D, and TRTVpIdiv all retain structure well; see the first row of Figure 3. In contrast, our method TRTVpIdiv can preserve clearer edges and simultaneously suppress the unnatural effects; see Figure 1(f). As we can see in Table 1, for the tested image SAR1, our method TRTVpIdiv outperforms the other compared methods. The values of ENL and EPI are consistently higher than those of the other compared methods, which show that the results produced by ours are more faithful to the clean images.

In Figure 2, we show and compare results for a real SAR image consisting of sharp edges and various homogeneous regions. Again, as can be seen, all the tested methods can remove the noise at this situation. However, DCA and TGV blur edges and homogeneous regions to varying degrees; see the corresponding zoomed views of Figure 2. Moreover, SARBM3D produces ghost artefacts in some homogeneous regions. In the corresponding ratio images, our method TRTVpIdiv shows the best result for retaining structures; see the second row of Figure 3. Again, our truncated method obtains better recovery with higher ENL and EPI values in Table 1. One important thing can be observed that, compared to the other methods, TRTVpIdiv yields more attractive results with edge preserving, homogeneous region smoothing, and contrast recovery.

In Table 1, the computation time of all the tested methods with the real SAR images are listed. Due to the multi-patch collaborative mechanism, the tested nonlocal methods (PPBit and SARBM3D) are computationally intensive. Compared to those nonlocal-based methods, the variational methods are less time-consuming, and our method TRTVpIdiv is the quickest one among these variational methods. The proposed method not only obtained better performance in suppressing speckle but also got the smallest computational complexity as well.

The above visual comparisons on the real SAR images show that our method TRTVpIdiv can produce better despeckling results than the compared methods in most cases. Specifically, our method TRTVpIdiv is noticeably better than all of the compared ones in terms of feature preserving and contrast recovery, especially in the case of the images including sharp features and homogeneous regions.

Table 1. Numerical evaluation results of SAR1 and SAR2.

	Index	Noisy	SARBM3D	PPBit	DCA	TGV	TRTVp
SAR1	ENL	20.30	80.43	205.09	177.32	157.68	224.75
	EPI	1	0.62	0.69	0.54	0.30	0.75
	Time(s)	–	126.24	63.49	36.12	40.98	15.25
SAR2	ENL	22.64	241.70	344.39	304.46	163.97	396.68
	EPI	1	0.50	0.64	0.42	0.33	0.66
	Time(s)	–	127.24	65.89	38.04	51.74	10.12

4. Conclusion

In this paper, we introduce a novel truncated nonconvex variational model for speckle suppression in SAR images. Compared to the traditional convex or smoothing model, the proposed model is more robust for recovering neat edges and preserving the SAR image contrast. An effective algorithm based on variable-splitting and ADMM is proposed to solve the model. Various numerical experiments show the efficiency of the proposed speckle suppression method.

Besides the speckle reduction application, we expect to extend our work to handle the wider class of problems, such as edge detection, texture and structure image decomposition, SAR images reconstruction.

Disclosure statement

The authors declare no conflicts of interest. Zheng Liu is the corresponding author.

Funding

This work was supported by the National Natural Science Foundation of China under Grant numbers 41701446, 41971356, 61702467, and CY119R015, the Zhejiang Provincial Natural Science Foundation of China under Grant number LQ20A010007, and the Post-doctoral Innovation Research Post of Hubei Province under Grant number 1232003.

ORCID

Chengde Han http://orcid.org/0000-0003-4295-3814

References

Aubert, G., and J.-F. Aujol. 2008. "A Variational Approach to Removing Multiplicative Noise." *SIAM Journal on Applied Mathematics* 68 (4): 925–946. doi:10.1137/060671814.

Buades, A., B. Coll, and J.-M. Morel. 2005. "A Review of Image Denoising Algorithms, with A New One." *Multiscale Modeling & Simulation* 4 (2): 490–530. doi:10.1137/040616024.

Chan, T., A. Marquina, and P. Mulet. 2000. "High-order Total Variation-based Image Restoration." *SIAM Journal on Scientific Computing* 22 (2): 503–516. doi:10.1137/S1064827598344169.

Chen, G., L. Gang, Y. Liu, X.-P. Zhang, and L. Zhang. 2019. "SAR Image Despeckling Based on Combination of Fractional-Order Total Variation and Nonlocal Low Rank Regularization." *IEEE Transactions on Geoscience and Remote Sensing* 58 (3): 2056–2070. doi:10.1109/TGRS.2019.2952662.

Dabov, K., A. Foi, V. Katkovnik, and K. Egiazarian. 2007. "Image Denoising by Sparse 3-D Transform-domain Collaborative Filtering." *IEEE Transactions on Image Processing* 16 (8): 2080–2095. doi:10.1109/TIP.2007.901238.

Deledalle, C.-A., L. Denis, and F. Tupin. 2009. "Iterative Weighted Maximum Likelihood Denoising with Probabilistic Patch-based Weights." *IEEE Transactions on Image Processing* 18 (12): 2661–2672. doi:10.1109/TIP.2009.2029593.

Dong, W., G. Shi, and X. Li. 2013. "Nonlocal Image Restoration with Bilateral Variance Estimation: A Low-rank Approach." *IEEE Transactions on Image Processing* 22 (2): 700–711. doi:10.1109/TIP.2012.2221729.

Feng, W., H. Lei, and Y. Gao. 2014. "Speckle Reduction via Higher Order Total Variation Approach." *IEEE Transactions on Image Processing* 23 (4): 1831–1843. doi:10.1109/TIP.2014.2308432.

Guan, D., D. Xiang, X. Tang, and G. Kuang. 2018. "SAR Image Despeckling Based on Nonlocal Low-rank Regularization." *IEEE Transactions on Geoscience and Remote Sensing* 57 (6): 3472–3489. doi:10.1109/TGRS.2018.2885089.

Guan, D., D. Xiang, X. Tang, and G. Kuang. 2019. "A SAR Image Despeckling Method Using Multi-Scale Nonlocal Low-Rank Model." *IEEE Geoscience and Remote Sensing Letters* 17 (3): 421–425.

He, Z., M. Deng, J. Cai, Z. Xie, Q. Guan, and C. Yang. 2020. "Mining Spatiotemporal Association Patterns from Complex Geographic Phenomena." *International Journal of Geographical Information Science* 34 (6): 1162–1187. doi:10.1080/13658816.2019.1566549.

Lanza, A., S. Morigi, and F. Sgallari. 2016. "Constrained TVp-L_2 Model for Image Restoration." *Journal of Scientific Computing* 68 (1): 64–91. doi:10.1007/s10915-015-0129-x.

Li, Z., Y. Lou, and T. Zeng. 2016. "Variational Multiplicative Noise Removal by DC Programming." *Journal of Scientific Computing* 68 (3): 1200–1216. doi:10.1007/s10915-016-0175-z.

Liu, J., T. Huang, G. Liu, S. Wang, and L. Xiaoguang. 2016. "Total Variation with Overlapping Group Sparsity for Speckle Noise Reduction." *Neurocomputing* 216: 502–513. doi:10.1016/j.neucom.2016.07.049.

Liu, J., T. Huang, I. W. Selesnick, L. Xiaoguang, and P. Chen. 2015. "Image Restoration Using Total Variation with Overlapping Group Sparsity." *Information Sciences* 295: 232–246. doi:10.1016/j.ins.2014.10.041.

Liu, J., T.-Z. Huang, X. Zongben, and L. Xiao-Guang. 2013. "High-order Total Variation-based Multiplicative Noise Removal with Spatially Adapted Parameter Selection." *Journal of the Optical Society of America. A, Optics and Image Science* 30 (10): 1956–1966. doi:10.1364/JOSAA.30.001956.

Liu, S., H. Qi, L. Pengfei, J. Zhao, M. Liu, and Z. Zhu. 2018. "Speckle Suppression Based on Weighted Nuclear Norm Minimization and Grey Theory." *IEEE Transactions on Geoscience and Remote Sensing* 57 (5): 2700–2708. doi:10.1109/TGRS.2018.2876339.

Lysaker, M., A. Lundervold, and X.-C. Tai. 2003. "Noise Removal Using Fourth-order Partial Differential Equation with Applications to Medical Magnetic Resonance Images in Space and Time." *IEEE Transactions on Image Processing* 12 (12): 1579–1590. doi:10.1109/TIP.2003.819229.

Meng, Y., Z. Zhou, Y. Liu, and Q. Luo. 2018. "Adaptive Pseudo-p-norm Regularization Based De-speckling of SAR Images." *Remote Sensing Letters* 9 (12): 1177–1185. doi:10.1080/2150704X.2018.1519268.

Parrilli, S., M. Poderico, C. V. Angelino, and L. Verdoliva. 2011. "A Nonlocal SAR Image Denoising Algorithm Based on LLMMSE Wavelet Shrinkage." *IEEE Transactions on Geoscience and Remote Sensing* 50 (2): 606–616. doi:10.1109/TGRS.2011.2161586.

Sattar, F., L. Floreby, G. Salomonsson, and B. Lovstrom. 1997. "Image Enhancement Based on a Nonlinear Multiscale Method." *IEEE Transactions on Image Processing* 6 (6): 888–895. doi:10.1109/83.585239.

Shi, Y., X. Zhang, Z. Rao, M. Wang, and M. Soleimani. 2019. "Reduction of Staircase Effect with Total Generalized Variation Regularization for Electrical Impedance Tomography." *IEEE Sensors Journal* 19 (21): 9850–9858.

Steidl, G., and T. Teuber. 2010. "Removing Multiplicative Noise by Douglas-Rachford Splitting Methods." *Journal of Mathematical Imaging and Vision* 36 (2): 168–184. doi:10.1007/s10851-009-0179-5.

Wu, C., Z. Liu, and S. Wen. 2018. "A General Truncated Regularization Framework for Contrast-preserving Variational Signal and Image Restoration: Motivation and Implementation." *Science China Mathematics* 61 (9): 1711–1732. doi:10.1007/s11425-017-9260-8.

Xiang, J., Y. Pengfei, L. Wang, and H. Mingqi. 2019. "A Novel Image-Restoration Method Based on High-Order Total Variation Regularization Term." *Electronics* 8 (8): 867. doi:10.3390/electronics8080867.

Xie, H., L. E. Pierce, and F. T. Ulaby. 2002. "SAR Speckle Reduction Using Wavelet Denoising and Markov Random Field Modeling." *IEEE Transactions on Geoscience and Remote Sensing* 40 (10): 2196–2212. doi:10.1109/TGRS.2002.802473.

Yu, W., Y. Zhang, A. Tinghua, Q. Guan, Z. Chen, and L. Haixia. 2020b. "Road Network Generalization considering Traffic Flow Patterns." *International Journal of Geographical Information Science* 34 (1): 119–149. doi:10.1080/13658816.2019.1650936.

Yu, W., Y. Zhang, A. Tinghua, and Z. Chen. 2020a. "An Integrated Method for DEM Simplification with Terrain Structural Features and Smooth Morphology Preserved." *International Journal of Geographical Information Science* 1–23. doi:10.1080/13658816.2020.1772479.